

10-28-2006

# Templated synthesis of gold-iron alloy nanoparticles using pulsed laser deposition

Won-Suk Chang

*Schools of Chemical Engineering and Biomedical Engineering, Purdue University, wchang@purdue.edu*

Jin-Won Park

*Purdue University*

Vijay Rawat

*Birck Nanotechnology Center, School of Materials Engineering, and School of Electrical and Computer Engineering, Purdue University, vijay.rawat@gmail.com*

Timothy D. Sands

*Purdue University, tsands@purdue.edu*

Gil U. Lee

*Birck Nanotechnology Center, Departments of Chemical and Biomedical Engineering, Purdue University, gl@atom.ecn.purdue.edu*

Follow this and additional works at: <http://docs.lib.purdue.edu/nanodocs>

---

Chang, Won-Suk; Park, Jin-Won; Rawat, Vijay; Sands, Timothy D.; and Lee, Gil U., "Templated synthesis of gold-iron alloy nanoparticles using pulsed laser deposition" (2006). *Other Nanotechnology Publications*. Paper 35.  
<http://docs.lib.purdue.edu/nanodocs/35>

This document has been made available through Purdue e-Pubs, a service of the Purdue University Libraries. Please contact [epubs@purdue.edu](mailto:epubs@purdue.edu) for additional information.

# Templated synthesis of gold–iron alloy nanoparticles using pulsed laser deposition

Won-Suk Chang<sup>1</sup>, Jin-Won Park<sup>1</sup>, Vijay Rawat<sup>2</sup>, Timothy Sands<sup>2</sup>  
and Gil U Lee<sup>1,3</sup>

<sup>1</sup> Schools of Chemical Engineering and Biomedical Engineering, Purdue University, Forney Hall of Chemical Engineering, West Lafayette, IN 47907, USA

<sup>2</sup> Schools of Materials Engineering and Electrical and Computer Engineering, Purdue University, MSEE building, West Lafayette, IN 47907, USA

E-mail: [gl@ecn.purdue.edu](mailto:gl@ecn.purdue.edu)

Received 16 May 2006, in final form 14 July 2006

Published 28 September 2006

Online at [stacks.iop.org/Nano/17/5131](http://stacks.iop.org/Nano/17/5131)

## Abstract

A means for synthesizing paramagnetic nanoparticles composed of an Au–Fe alloy is described using pulsed laser deposition (PLD) of the alloy into a mesoporous alumina membrane template. Nanoparticles  $46 \pm 13$  nm in diameter and composed of a 17% Fe alloy have been created by depositing a 35% Fe alloy into a template with 65 nm diameter pores. These paramagnetic nanoparticles had a saturation magnetization of  $11.5 \text{ emu g}^{-1}$  at 2000 G, and their UV–visible extinction spectrum was dominated by strong absorption similar to that of  $\text{Fe}_3\text{O}_4$  nanoparticles. The surfaces of these nanoparticles were readily functionalized with a dense monolayer of DNA oligonucleotides that had a 5' thiol group. The Au–Fe nanoparticles appear to be well suited for biotechnological applications and single molecule measurements as they can be synthesized in a specific size range, are strongly paramagnetic, and may be easily functionalized with biological macromolecules.

(Some figures in this article are in colour only in the electronic version)

## 1. Introduction

Paramagnetic particles are being used in an increasing number of biotechnologies that include drug delivery [1], *in vivo* imaging [2], hyperthermia therapy [3], diagnostics [4], bioanalytical measurements [5–7], and affinity separation of cells, viruses, and biological macromolecules [8–13]. The particles used in these applications need to be stable in salt solutions, uniform in size, and responsive to magnetic fields that are produced by small permanent magnets. The micron-size particles that are currently used for separation applications are typically composed of assemblies of superparamagnetic nanoparticles of magnetite or maghemite distributed in a polymer matrix [14–19]. The polymer matrix stabilizes the colloidal particles in aqueous solution and provides chemical groups that can be conjugated to proteins and polynucleotides. An inherent limitation of these iron oxide nanoparticle composites is that they have a relatively low magnetization and

will ultimately degrade due to the decomposition of magnetite to a nonmagnetic ferrite [20–22].

Core–shell and alloy nanoparticles have recently been synthesized that appear to overcome some of the limitations of iron oxides. Zhong *et al* [23] have synthesized  $\text{Fe}_3\text{O}_4$  core–Au shell structures by forming an Au shell on a  $\text{Fe}_3\text{O}_4$  core particle. These nanoparticles were designed to be magnetic and chemically stabilized by the Au shell. Unfortunately, in our experience it appears that the Au shell forms a poor diffusion barrier which we attribute to the high density of grain boundaries in the Au shell. It can also be difficult to synthesize these particles due to the need to conduct the gold coating step in reagents that destabilize colloidal sols. Fe–Pt alloy nanoparticles have recently been synthesized by Sun *et al* [24] that appear have a very narrow size distribution and a surface chemistry similar to that of pure Pt. Unfortunately, these particles are not suitable for bioseparation as they appear to have ferromagnetic properties.

Metal and semiconductor nanowires have been created using templated deposition of material by the electrodeposition

<sup>3</sup> Author to whom any correspondence should be addressed.

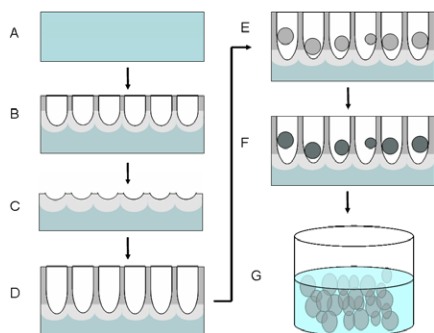


**Figure 1.** Process used to create the Au–Fe alloy nanoparticles. (A)–(D) A mesoporous alumina template was synthesized by electrochemical oxidation. (E) PLD deposition of the Au–Fe alloy in the nanoporous template. (F) The template was then heated to 650 °C for 3 h in an Ar/H<sub>2</sub> environment. (G) The nanoparticles were released from the template by removal of the alumina matrix.

in mesoporous alumina [25–29]. In this process, mesoporous alumina is created by the anodic oxidation of aluminium in acidic solutions that results in densely packed and highly uniform nanometre-sized pores [30, 31]. These 20–200 nm pores can be grown to depths of 10–100  $\mu\text{m}$ . Electrodeposition of metals in the mesoporous alumina produces highly uniform cylindrical wires 20–200 nm in diameter and microns in length. Recently, magnetic nickel wires have been created by this templated synthesis approach [32].

In this paper we describe the templated synthesis of magnetic nanoparticles of an Au–Fe alloy using PLD deposition of the material into a mesoporous alumina matrix. Au–Fe alloys have a well defined phase behaviour and are known to form both a gold-rich fcc solid solution (Au) and iron-rich bcc solid solution ( $\alpha\text{Fe}$ ) [33–35]. At low iron compositions the (Au) alloy is the predominant phase formed if the material is quenched to room temperature. This material is known to have spin glass or micromagnetic magnetic properties, i.e., it is paramagnetic at room temperature but has a freezing temperature at which the spins freeze but do not have long-range order [36]. PLD was selected as a means of deposition for the alloy in the mesoporous alumina, rather than electron beam deposition or electrodeposition, to avoid the phase separation during the deposition process. The physical and chemical properties of these particles were characterized using transmission electron spectroscopy (TEM), UV–vis spectroscopy, and magnetometry. The fact that these particles can be synthesized over a wide size range, are strongly paramagnetic, and can be easily functionalized makes them excellent candidates for bioanalytical applications.

## 2. Experimental details

The Au–Fe alloy nanoparticles were created using the three-step process outlined in figure 1. The mesoporous alumina templates were first prepared by anodic oxidation [31]. The 99.9987% pure, 200  $\mu\text{m}$  thick aluminium sheets (Aldrich, Milwaukee, WI) were prepared for oxidation by degreasing in acetone (ACS grade, Aldrich, Milwaukee, WI) for 15 min followed by electropolishing in a 50/50 by volume ratio solution of ethanol/perchloric acid at 14 V for 15 min. A

first anodization was carried out in 0.3 M oxalic acid (ACS grade, Aldrich, Milwaukee, WI) solution for 10 h at 40 V. The anodized layer was released by reaction with a 0.15 M phosphoric acid (ACS grade, Alfa-Aesar, Ward Hill, MA) and 0.15 M chromic acid (ACS grade, Alfa-Aesar, Ward Hill, MA) solution for 15 min at 70 °C. The second anodization was performed at the same conditions as the first anodization but was carried out for 5 h to produce pores 30  $\mu\text{m}$  in depth. Pore widening was performed in 0.5 M phosphoric acid for 35 min at room temperature. Field emission scanning electron microscopy (Hitachi S4800, Hitachi High-Technologies Corp., Berkshire, UK) of these surfaces revealed highly ordered arrays of pores 60–70 nm diameter. In the second step, PLD of the Au–Fe alloy was carried out with a commercial system (PVD Product Inc., Wilmington, MA) equipped with a 248 nm KrF excimer laser (Lambda Physik USA, Ft. Lauderdale, FL). A 65%–35% Au–Fe alloy target was prepared by arc melting and quenching the metals at  $10^{-5}$  Torr vacuum (Model 5SA Centorr Vacuum Inc., Nashua, NH). The alloyed particles were deposited within the mesoporous anodized template at a chamber base pressure of  $5 \times 10^{-7}$  Torr with a laser pulse frequency of 5 Hz and a laser fluence of  $3 \text{ J cm}^{-2}$  for 2 h. The distance from the alloyed target to the anodized Al template was 15 cm. The nanoparticles were then annealed in the alumina matrix at 650 °C for 3 h in an atmosphere of 5% hydrogen and 95% argon. In the last step, this template was immersed in a 0.5 M NaOH solution (ACS grade, Alfa-Aesar, Ward Hill, MA) for 2 h to isolate the Au–Fe alloy particles from the template. The nanoparticles were separated from the NaOH solution with a permanent magnet, washed with 0.5 M NaOH, and resuspended in UVO milli-Q water (Millipore, Bedford, MA).

Electron microscopy was used to study the structure and composition of the nanoparticles formed by the PLD templated synthesis process. A CM12 TEM (Philips Electron Optics, Eindhoven, Netherlands) was used to study these particles at a 120 kV accelerating voltage with a resolution of 0.34 nm.

## 3. Results

### 3.1. Morphology of the Au–Fe alloy nanoparticles

Figure 2(A) presents transmission images of the as-deposited nanoparticles which had a fairly broad distribution of sizes and were irregular in shape. After annealing at 650 °C the shape of the particles became more regular, as shown in figure 2(B), with few small particles observed. The average diameter of the annealed nanoparticle was  $46 \pm 13$  nm, but a histogram of the measured particle diameters, figure 2(C), reveals that the diameters were either centred about 55 nm in diameter or distributed between 20 and 40 nm. This size distribution suggests that the PLD process naturally produces particles of a mean diameter of 55 nm which we would expect from an alumina template with 65 nm diameter pores. We believe that the ‘line-of-sight’ nature of PLD leads to the production of the smaller particles due to the deposition of the alloy on the walls of the pores that are not aligned with the PLD deposition axis. The change in shape and size of the nanoparticles after annealing then appears to result from the coalescence of the alloy that is driven by a lower interfacial free energy.

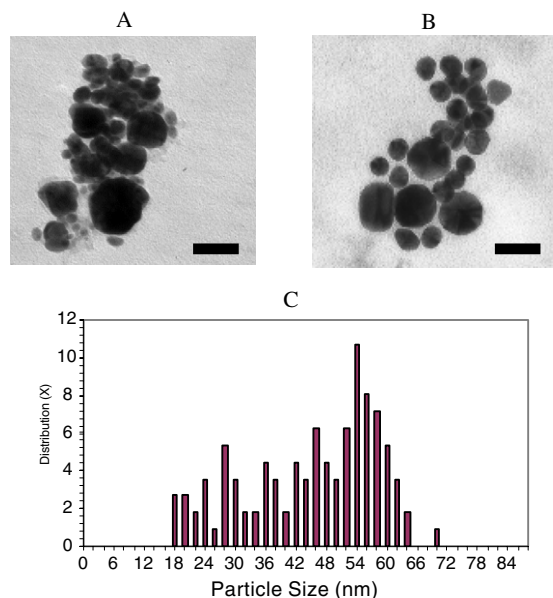


**Figure 2.** Transmission electron micrographs of the Au–Fe alloy nanoparticles produced by templated synthesis. (A) Micrograph of the as-deposited nanoparticles with a 50 nm scale bar. (B) Micrograph of the nanoparticles after annealing. (C) Histogram of the diameters of the nanoparticles after annealing.

Selected area electron beam diffraction patterns were simultaneously measured on the annealed Au–Fe alloy nanoparticles and 40 nm gold nanoparticles purchased from BBInternational (Cardiff, UK). Figure 3 presents the electron beam diffraction patterns from the alloy (left) that were indexed with the gold diffraction pattern (right). The alloy pattern clearly indicates that the intermetallic nanoparticles have an fcc crystal structure with a lattice parameter similar to that of gold. This is consistent with previous studies of quenched Au–Fe alloy at room temperature in which the fcc (Au) phase is observed to form at iron compositions less than 60% [36, 37]. The calculated lattice parameter for the Au–Fe intermetallic phase was  $4.0312 \pm 0.0507 \text{ \AA}$ . The lattice parameters of bulk (Au) alloys have been characterized for 15.7% and 20% Fe using x-ray diffraction and found to be 4.0358 and 3.995  $\text{\AA}$ , respectively [37, 38]. Application of Vegard's Law within this range indicates that the (Au) alloy is composed of 17% Fe [36]. However, the phase behaviour of the (Au) alloy leads us to predict that the nanoparticles should be composed of 35% Fe if there were a direct transfer of material from the target to the nanoparticles [38]. We believe that the Fe depletion is a result of removal of iron from the surface of the nanoparticles during the alumina etching step.

### 3.2. Optical properties

The UV–visible extinction spectra of the Au–Fe alloy nanoparticles and several reference materials were measured with a spectrophotometer (EZ lambda, Perkin Elmer, Boston, MA). Figure 4 presents the extinction spectra of  $10^9$  Au–Fe particles  $\text{ml}^{-1}$ ,  $2 \times 10^{13}$  Au particles  $\text{ml}^{-1}$ , and  $10^{11}$   $\text{Fe}_3\text{O}_4$  particles  $\text{ml}^{-1}$ . It is clear that the Au–Fe nanoparticles strongly attenuate the transmitted light intensity

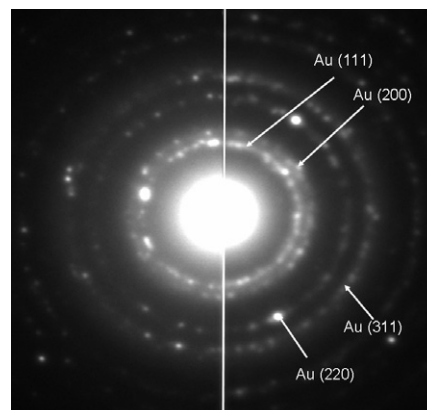


**Figure 3.** Electron diffraction patterns of Au–Fe alloyed nanoparticles prepared by PLD (left) and pure Au 40 nm nanoparticle (right).

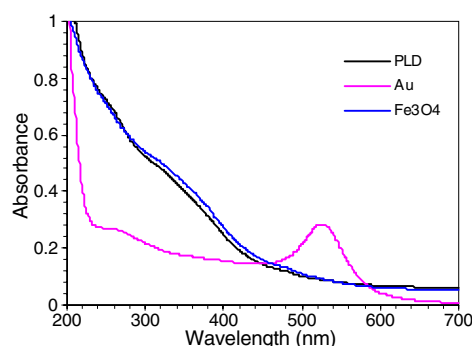


**Figure 4.** Adsorption spectra of the Au–Fe alloy nanoparticles, 20 nm Au colloidal particles purchased from BBInternational, and 5–20 nm  $\text{Fe}_3\text{O}_4$  colloidal particles.

between 260 and 450 nm. The  $1/\lambda$  functional behaviour of the extinction spectra suggests the optical activity of the Au–Fe nanoparticles is dominated by absorption and not scattering. It is clear that the Au–Fe nanoparticles' extinction spectrum is very similar to that of the  $\text{Fe}_3\text{O}_4$  nanoparticles and that a surface plasmon resonance peak is not observed that would be characteristic of Au nanoparticles [38]. To our knowledge this is the first time that the optical properties of Au–Fe alloy nanoparticles have been measured. This measurement appears to confirm that the electronic properties of the Au–Fe alloy nanoparticles differ from those of Au and that Au nanoparticles are not present in the Au–Fe nanoparticle suspension.

### 3.3. Magnetic properties

The magnetic properties of the Au–Fe alloy nanoparticles were measured using a form of vibrating reed magnetometry (nVSM) that allows measurements to be made on nanogram quantities of samples. In this technique, the magnetic moment of the magnetic material was sensed with a microfabricated force transducer as an external magnetic field and field gradient were applied to the material. The force ( $F$ ) generated by a volume of magnetic material  $V$  is related to the magnetization

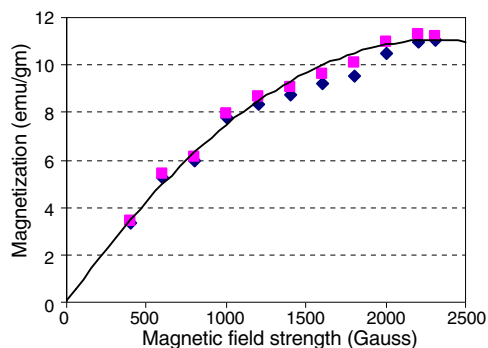


**Figure 5.** Magnetic field strength of the alloyed particles.

of the material  $M(B)$  through the equation

$$\vec{F} = M(B)V \frac{d\vec{B}}{dz}$$

where  $\frac{d\vec{B}}{dz}$  is the magnetic field gradient. This force was measured with an atomic force microscope equipped with an ultralow noise optical lever detector (3D Molecular Force Probe, Asylum Research, Santa Barbara, CA) using a silicon oxynitride AFM cantilever (Olympus, Tokyo, Japan). The spring constant for the microfabricated cantilever was carefully independently determined from a shift in resonance frequency of the first mode of the cantilever under a known added mass

$$m = \frac{k}{4\pi^2} \left( \frac{1}{\nu_0^2} - \frac{1}{\nu_1^2} \right)$$

where  $m$  is the mass of a quartz microparticle that was added to the cantilever,  $k$  is the spring constant of the cantilever, and  $\nu_0$  and  $\nu_1$  are the resonance frequencies of the cantilever before and after the mass was added, respectively [39]. A mass of approximately 300 ng of dried nanoparticles was then attached to the end of the cantilever using approximately 0.3 ng of UV-sensitive epoxy. The magnetization curve of the material was determined by moving the AFM cantilever toward a rectangular 0.5 inch  $\times$  0.5 inch  $\times$  0.125 inch neodymium iron boron permanent magnet whose field was carefully mapped using a Hall probe (GMW, San Carlos, CA). The accuracy of this technique was limited by the force sensitivity of the AFM and is  $\pm 0.1$  emu  $g^{-1}$ .

Figure 5 presents the magnetization properties of the Au–Fe alloy nanoparticles measured with nVSM. It is clear that the forward and retraction magnetization curves were indistinguishable within the resolution of the technique, which is consistent with the paramagnetic behaviour that we would expect to observe in Au–Fe alloys at room temperature. That is, magnetization measurements of the bulk (Au) phase have demonstrated that the Curie temperature of the 20% Fe alloy is 200 K [39]. The saturated magnetization of the Fe–Au alloy nanoparticles was 11.5 emu  $g^{-1}$  and saturation was reached at approximately 2000 G. The moment of individual Fe atoms in the nanoparticles were determined to be  $2.3 \mu_B$  from the Curie constant. This Fe moment is smaller than that of bulk Au–Fe alloys, which range from  $3.4 \mu_B$  for 15% Fe to  $3.76 \mu_B$  for 18% Fe [40, 41]. Magnetization measurements on the bulk fcc solid solution phase (Au) have demonstrated it is very

stable even at elevated temperatures, i.e. no detectable  $\alpha$ Fe precipitation was detected after heating this phase to 200 °C for 200 h [40]. However, bulk alloys have demonstrated a gradual increase of susceptibility at longer times, which has been attributed to the formation of Fe-rich, two-atom-thick platelets in alloys with 14–19% Fe [42]. The Au–Fe alloy nanoparticles have been stored and used in this laboratory for up to six months with no observed change in their magnetophoretic mobility.

#### 3.4. Surface modification with thiol-modified DNA oligonucleotide

The surfaces of the Au–Fe nanoparticles were functionalized by reaction with a thiolated DNA oligonucleotide [43]. The DNA oligonucleotide that was used had the sequence CGCATTTCAGGAT and was 5' labelled with a hexamethyl-capped thiol and 3' labelled with fluorescein (FAM<sup>®</sup>). This HPLC purified and MALDI analysed oligonucleotide was acquired from a commercial source (Integrated DNA Technologies, Coralville, IA). The Au–Fe nanoparticles were modified with this oligonucleotide after deprotection of the thiol with dithiothreitol and careful separation using size exclusion chromatography. Solutions of 1  $\mu$ M oligonucleotide were reacted with  $\sim 10^{12}$  particle  $ml^{-1}$  for 20 h in 10 mM phosphate buffer (at pH 7.0) and then 40 h in 100 mM phosphate buffer. The total oligonucleotide density on the nanoparticles was determined by displacing them with 25 mM mercaptoethanol (Aldrich, Milwaukee, WI, 98%) for 24 h, which has been shown to completely replace thiolated oligonucleotide-immobilized Au [43]. The fluorescence signal from the fluorescein-labelled DNA was then measured in the free effluent using a fluorometer (LS 50B, Perkin Elmer, Wellesley, MA) with excitation wavelength at 480 nm and emission wavelength at 530 nm. The surface area of the Au–Fe nanoparticles was determined by calculating a mean area from all the particle diameters measured by TEM. The DNA surface coverage for the Au–Fe nanoparticles was determined to be  $1.2 \times 10^{13}$   $cm^{-2}$ , which is in reasonable agreement with the  $2.0 \times 10^{13}$   $cm^{-2}$  coverage measured for Au nanoparticles prepared under identical conditions. These results are also in reasonable agreement with the previously reported values ranging between  $2.0 \times 10^{12}$  and  $9.0 \times 10^{13}$   $cm^{-2}$  depending on the length and the sequence of the DNA [43].

## 4. Conclusion

In summary, we have demonstrated for the first time that Au–Fe alloy nanoparticles can be synthesized by PLD deposition of the alloy in a mesoporous alumina template. The average nanoparticle size obtained by depositing the alloy in 60–70 nm pores was  $46 \pm 13$  nm. The advantage of using templated-PLD synthesis is that the alloy structure is maintained and the size of the particle may be varied across a range that is typically difficult to achieve with traditional solution-based chemistry. The distribution of particle sizes was broadened due to the line-of-sight nature of PLD but the influence of this effect can be minimized by coalescing the particles through annealing at 650 °C. The composition of the nanoparticle was determined to be 17% Fe, which was lower than that of the

35% Fe composition of the target. We attribute this loss in iron to the etching of the alumina membrane, which is a process that will also remove any iron that is distributed in near the surface of the nanoparticle. The nanoparticles formed a gold-rich fcc phase in which iron atoms were distributed, which is consistent with previous reports of the behaviour of bulk Au-Fe alloys. The optical activity of the Au-Fe nanoparticles was found to be dominated by absorption, and the extinction spectrum was very similar to that of Fe<sub>3</sub>O<sub>4</sub> nanoparticles. The Au-Fe nanoparticles showed paramagnetic properties at room temperature with a saturation magnetization of 11.5 emu g<sup>-1</sup> at 2000 G. Reaction with thiolated DNA oligonucleotides produced a dense monolayer on the Au-Fe nanoparticles and suggests that the particles react with thiol in a manner similar to that of gold.

The Au-Fe nanoparticles appear to be well suited for biotechnological applications and single molecule measurements as they can be synthesized in a specific size range, are strongly paramagnetic, and may be easily functionalized with biological macromolecules. We believe that this is the first application of a superparamagnetic particle to bioseparation that is smaller than 100 nm. These particles should be able to react rapidly with biological macromolecules due to their high diffusion rates. Iron oxide nanoparticles have not been used for bioseparation as they become ferromagnetic at approximately 30 nm and this size particle has a very low mobility. A potential limitation of the templated synthesis technique is the cost of the fabrication of the nanoporous membrane template and PLD deposition. We estimate that 10<sup>11</sup> nanoparticles can be produced on a 3 inch diameter template with yield of approximately 50%. This suggests that templated synthesis appears to be a viable approach to nanoparticle synthesis although the capital costs associated with PLD deposition are not insignificant.

## Acknowledgments

This work has been funded by the NASA Institute for Nanoelectronics and Computing (NASA NCC 2-1363). We would like to acknowledge Deborah Sherman of the School of Agriculture, Purdue University, for her technical assistance with the FE-SEM and Patricia Metcalf of the School of Materials Engineering, Purdue University, for her technical assistance with the preparation of the Au-Fe alloy PLD target. We would also like to thank Kyung Jae Jeong, Sang Won Lee, and Ronald Andres and for their valuable comments.

## References

- [1] Devineni D, Blanton C D and Gallo J M 1995 *Bioconjug. Chem.* **6** 203–10
- [2] Dodd C H *et al* 2001 *J. Immunol. Methods* **256** 89–105
- [3] Lao L L and Ramanujan R V 2004 *J. Mater. Sci. Mater. Med.* **15** 1061–4
- [4] Baselt D R, Lee G U, Natesan M, Metzger S W, Sheehan P E and Colton R J 1998 *Biosens. Bioelectron.* **13** 731–9
- [5] Shang H, Kirkham P M, Myers T M, Cassell G H and Lee G U 2005 *J. Magn. Magn. Mater.* **293** 382–8
- [6] Strick T R, Allemand J F, Bensimon D, Bensimon A and Croquette V 1996 *Science* **271** 1835–7
- [7] Smith S B, Finzi L and Bustamante C 1992 *Science* **285** 1122–6
- [8] Kemshead J T, Ugelstad J, Rembaum A and Gibson F 1982 *Eur. J. Cancer Clin. Oncol.* **18** 1043–3
- [9] Dirami G, Poulter L W and Cooke B A 1991 *J. Endocrinol.* **130** 357–65
- [10] Ahmed A R H, Olivier G W J, Adams G, Erskine M E, Kinsman R G, Branch S K, Moss S H, Notarianni L J and Pouton C W 1992 *Biochem. J.* **286** 377–82
- [11] Ito T, Smith C L and Cantor C R 1992 *Proc. Natl Acad. Sci. USA* **89** 495–8
- [12] Wahlberg J, Holmberg A, Bergh S, Hultman T and Uhlen M 1992 *Electrophoresis* **13** 547–51
- [13] McConnell S J, Dinh T, Le M H and Spinella D G 1999 *Biotechniques* **26** 208–14
- [14] Moller W, Scheuch G, Sommerer K and Heyder J 2001 *J. Magn. Magn. Mater.* **225** 8–16
- [15] Stevenson J P, Rutnakornpituk M, Vadala M, Esker A R, Charles S W, Wells S, Dailey J P and Riffle J S 2001 *J. Magn. Magn. Mater.* **225** 47–58
- [16] Khng H P, Cunliffe D, Davies S, Turner N A and Vulfson E N 1998 *Biotechnol. Bioeng.* **60** 419–24
- [17] Rana S, White P and Bradley M 1999 *Tetrahedron Lett.* **40** 8137–40
- [18] Ramirez L P and Landfester K 2003 *Macromol. Chem. Phys.* **204** 22–31
- [19] Bizdoaca E L, Spasova M, Farle M, Hilgendorff M and Caruso F 2002 *J. Magn. Magn. Mater.* **240** 44–6
- [20] Liu X Q, Guan Y P, Ma Z Y and Liu H Z 2004 *Langmuir* **20** 10278–82
- [21] Zheng W M, Gao F and Gu H C 2005 *J. Magn. Magn. Mater.* **288** 403–10
- [22] Devineni D, Blanton C D and Gallo J M 1995 *Bioconjug. Chem.* **6** 203–10
- [23] Wang L, Luo J, Maye M M, Fan Q, Rendeng Q, Engelhard M H, Wang C, Lin Y and Zhong C-J 2005 *J. Mater. Chem.* **15** 1821–32
- [24] Sun S, Murray C B, Weller D, Folks L and Moser A 2000 *Science* **287** 1989–92
- [25] Hornyak G L, Patrissi C J and Martin C R 1997 *J. Phys. Chem. B* **101** 1548–55
- [26] Martin C R 1996 *Chem. Mater.* **8** 1739–46
- [27] Hoyer P 1996 *Adv. Mater.* **8** 857–9
- [28] Sander M S and Tan L S 2003 *Adv. Funct. Mater.* **13** 393–7
- [29] Prieto A L, Sander M S, Martin-Gonzalez M S, Gronsky R, Sands T and Stacy A M 2001 *J. Am. Chem. Soc.* **123** 7160–1
- [30] Li F, Zhang L and Metzger R M 1998 *Chem. Mater.* **10** 2470–80
- [31] Masuda H and Sotoh M 1996 *Japan. J. Appl. Phys.* **35** L126–9
- [32] Yin A J, Li J, Bennett A J and Xu J M 2001 *Appl. Phys. Lett.* **79** 1039–41
- [33] Jette E R, Bruner W L and Foote F 1934 *Trans. Metall. AIME* **111** 354–9
- [34] Pan S T, Kaufmann A R and Bitter F 1942 *J. Chem. Phys.* **10** 318–21
- [35] Raub E and Walter P 1950 *Z. Metallk.* **41** 234–8
- [36] Crangle J and Scott W R 1965 *J. Appl. Phys.* **36** 921–8
- [37] Kubaschewski O and Ebert H 1944 *Z. Elektrochem. Angew. Phys. Chem.* **50** 138–44
- [38] Turkevich J, Garton G and Stevenson P C 1954 *J. Colloid Sci.* **8** S26–35
- [39] Cleveland J P, Manne S, Bocek D and Hansma P K 1993 *Rev. Sci. Instrum.* **64** 403–5
- [40] Scheil E, Specht H and Wachtel E 1958 *Z. Metallk.* **49** 590–600
- [41] Beck P A 1980 *Solid State Commun.* **34** 581–6
- [42] Dartyge E, Bouchiat H and Monod P 1982 *Phys. Rev. B* **25** 6995–7002
- [43] Demers L M, Mirkin C A, Mucic R C, Reynolds R A, Letsinger R L, Elghanian R and Viswanadham G 2000 *Anal. Chem.* **72** 5535–41